Communication

Single-Cut Phaseless Near-Field Measurements using Two Probes

Fernando Rodríguez Varela, Jorge Calatayud Maeso, Xiaoliang Sun,
Belén Galocha Iragüen and Manuel Sierra Castañer

***Abstract*—Single-cut phaseless measurements enable the testing of antenna devices with no reference channel by measuring and transforming to far-field individual pattern cuts. This typically requires performing two single-cut measurements at different distances which may be infeasible or too time consuming in some antenna facilities. As an alternative, this communication proposes the use of a two-probe system connected to the same coherent receiver. The relative phase between probes is exploited to retrieve the absolute phase using a state-of-the-art linearized phase retrieval approach. Simulations and measurements are performed to validate the technique which includes an innovative probe-to-probe calibration method.**

***Index Terms*—Amplitude-only, multi-probe, fast measurements, phaseless, single-cut.**

I. Introduction

Single-cut antenna measurements [1]–[4] are a popular time-saving alternative to conventional near-field spherical or cylindrical approaches [5]–[7]. From the near-field of the antenna under test (AUT) in a cardinal cut (typically the E and H planes), the radiation pattern over that plane is extrapolated. Drastic reductions in measurement time are obtained since the scanning of the full spherical or cylindrical surfaces is avoided. The approximation errors are very low for antennas with separability of the aperture fields, typically array and reflector antennas. In all these processing steps, the phase information remains necessary to perform the far-field transformation.

The measurement of the phase signal in standard passive antennas is no longer an issue with the wide availability of vectorial measurement equipment. Nevertheless, the topic of phaseless measurements has experienced a resurgence due to the increasing presence of highly integrated and active antennas, where the extraction of a physical phase reference channel is unfeasible. This issue can be circumvented with the use of an auxiliary antenna which creates a phase reference [8], but in most cases it forces the AUT to be stationary to keep a stable reference channel.

Some efforts have been made to implement single-cut phaseless measurement techniques [9]–[11]. This has been made possible by the application of the two-scans technique of the more traditional spherical [12], [13] or planar [14] phaseless measurements. If the radiated near-field magnitude is measured in two concentric and coplanar cuts it is possible to extrapolate the phase with an iterative algorithm. Nevertheless, the process of changing the AUT-to-probe distance can be extremely time consuming or even infeasible for some measurement facilities.

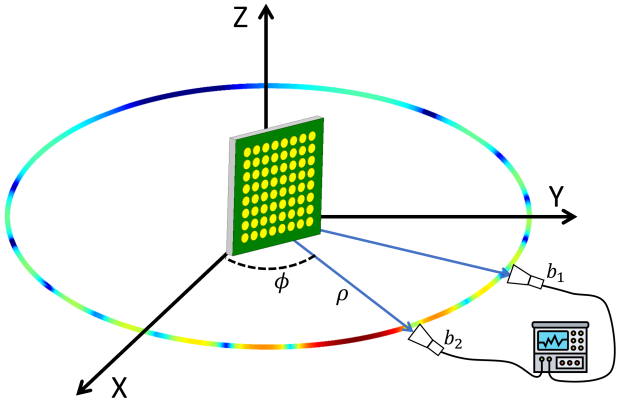

Fig. 1. Geometry of the proposed antenna measurement concept.

Two-scans phaseless measurements can be avoided by making use of the partial coherence information provided by multi-probe systems. The relative phase between probe signals is combined with the measured magnitude to retrieve the complete near-field phase. The earliest approaches were based on the concatenation of phase differences between measurement pairs [15], [16], which imposed some practical limitations related to positioning accuracy and error propagation. Moreover, the manufacturing and testing of dedicated microwave circuits was needed to extract the partial coherent signals. Consequently, a novel and flexible methodology has recently been introduced, wherein the phase retrieval problem is reformulated as a linearized minimization, showcasing successful recovery guarantees [17]–[19]. Such methodology leverages the phase coherence between ports of microwave receivers, avoiding the need of interferometric microwave circuitry. However, channel balance calibration issues may complicate the practical implementation of such approaches.

The present communication focuses on the application of linearized phase retrieval to single-cut phaseless measurements with reduced hardware requirements. It has been implemented by measuring the near-field of a reference-less AUT with a coherent two-probe system, as depicted in Fig. 1. This study reveals the significant influence of spatial and electrical mismatches between probes on the efficacy of the linearization of the problem. To address this concern, a pioneering probe-to-probe calibration technique is introduced. As a result, the need for identical probes or specialized microwave circuitry is eliminated [15], [16]. The feasibility of the proposed technique is demonstrated through successful full phaseless measurements using a straightforward probe arrangement that can be easily replicated in most measurement facilities.

Manuscript received November 24, XX; revised May 8, XX; accepted May 29, XX. Date of publication June 25, XX; date of current version December 16, XX.

This work was funded by MCIN/AEI/10.13039/501100011033 and by the European Union "NextGenerationEU"/PRTR" under the proyect TED2021-131975A-I00 (ANTHEM5G).

Fernando Rodríguez Varela is with the Microwave Engineering and Radiocommunication Systems Group, Universidad Rey Juan Carlos de Madrid, Fuenlabrada, Spain.

Jorge Calatayud Maeso, Xiaoliang Sun, Belén Galocha Iragüen, and Manuel Sierra Castañer are with the Information Processing and Telecommunications Center, Radiation Group, Department of Signals, Systems and Radiocommunications, ETSI Telecomunicación, Universidad Politécnica de Madrid, 28040 Madrid, Spain (e-mail: belen@gr.ssr.upm.es).

Color versions of one or more figures in this article are available at https://doi.org/10.1109/TAP.2021.3090846. Digital Object Identifier 10.1109/TAP.2021.3090846

II. Theoretical background

A. Single-cut near-field to far-field transformation

The near-field measurement scenario of Fig. 1 with cylindrical coordinates (ρ, ϕ, z) is considered. The tangential components of the electric field radiated by the AUT can be expanded in elementary cylindrical waves [5]. However, in the single-cut methodology, the measurement is only performed for a $z = 0$ cut, which can be considered a cylinder of infinitesimal height, leading to the following expansion [4]:

$$E_z(\rho,\phi) = \sum_{n=-N}^{N} k c_n H_n^{(2)}(k\rho) e^{jn\phi} \tag{1}$$

$$E_\phi(\rho,\phi) = -\sum_{n=-N}^{N} d_n \frac{\partial H_n^{(2)}(k\rho)}{\partial \rho} e^{jn\phi} \tag{2}$$

being E_z and E_ϕ the tangential components of the radiated field, $H_n^{(2)}$ the Hankel funcion of second kind and k the free space wave number. The terms c_n and d_n are single-cut wave coefficients (SCWC) and are closely related to the cylindrical wave coefficients [5] but in one dimension.

Without loss of generality we focus now in the E_z component of the field. If this polarization is measured at M sampling positions with two different probes, (1) can be expressed in a discretized way:

$$\boldsymbol{b_1} = \boldsymbol{H_1 c_n} \tag{3}$$

$$\boldsymbol{b_2} = \boldsymbol{H_2 c_n} \tag{4}$$

where $\boldsymbol{c_n}$ is a column vector of size $2N+1$ containing all c_n coefficients of the AUT. Vectors $\boldsymbol{b_1}$ and $\boldsymbol{b_2}$ are formed by the near-field samples of the first and second probe. Each of them is of size $M > 2N+1$, to introduce some oversampling. Matrices $\boldsymbol{H_1}$ and $\boldsymbol{H_2}$ are of size $M \times (2N+1)$ and they perform the Fourier summations in (1). Finally, (3) and (4) are grouped into a single equation:

$$\begin{bmatrix} \boldsymbol{b_1} \\ \boldsymbol{b_2} \end{bmatrix} = \begin{bmatrix} \boldsymbol{H_1} \\ \boldsymbol{H_2} \end{bmatrix} \boldsymbol{c_n} \quad \Longrightarrow \quad \boldsymbol{b} = \boldsymbol{H c_n} \tag{5}$$

B. Single-cut phaseless algorithm

If the AUT lacks a reference channel, only the magnitude signals $|\boldsymbol{b_1}|$ and $|\boldsymbol{b_2}|$ can be measured. Their corresponding phase components, $\boldsymbol{\psi_1} = \boldsymbol{e^{j\angle b_1}}$ and $\boldsymbol{\psi_2} = \boldsymbol{e^{j\angle b_2}}$, respectively, become the unknowns of the phaseless problem. When both probes are connected to the same receiver it is possible to extract the relative phase between them: $\boldsymbol{\psi_{2,1}} = \boldsymbol{e^{j\angle b_2}/e^{j\angle b_1}}$. The introduced vectors meet the following identity [17]:

$$\begin{bmatrix} \boldsymbol{b_1} \\ \boldsymbol{b_2} \end{bmatrix} = \begin{bmatrix} D(|\boldsymbol{b_1}|) \\ D(|\boldsymbol{b_2}| \otimes \boldsymbol{\psi_{2,1}}) \end{bmatrix} \boldsymbol{\psi_1} \quad \Longrightarrow \quad \boldsymbol{b} = \boldsymbol{B\psi_1} \tag{6}$$

where $\otimes$ denotes element-wise multiplication and $D()$ returns a square diagonal matrix with the elements of the vector inside the brackets on the main diagonal.

Using this notation an homogeneous linear system of equations is defined [17]:

$$\left(\boldsymbol{I} - \boldsymbol{H}\boldsymbol{H}^{\dagger}\right) \boldsymbol{B\psi_1} = 0 \quad \Longrightarrow \quad \boldsymbol{R\psi_1} = 0 \tag{7}$$

where † computes the pseudo-inverse and $\boldsymbol{I}$ is the identity matrix. $\boldsymbol{H}\boldsymbol{H}^{\dagger}$ can be regarded as electromagnetic filter acting over the near-field vector $\boldsymbol{b}$ which cancels field variations incompatible with the SCWC of the AUT. Signal variations with harmonic order higher than N will be filtered out. To maximize the filtering capabilities of this operator, the center of the expansion in (1-2) is selected so that N becomes minimal. The solution vector $\boldsymbol{\psi_1}$ will be the one that generates a vector $\boldsymbol{b}$ which is unaffected by the electromagnetic filter. After the missing phases $\boldsymbol{\psi_1}$ have been retrieved, the complex near-field of both probes can be reconstructed and transformed to far-field using standard single-cut methods [4]. Finally, the average of both patterns can be computed to reduce measurement uncertainties.

C. SVD analysis and solution of the system

The conditioning of (7) can be studied computing the Singular Value Decomposition (SVD) of $\boldsymbol{R} = \boldsymbol{USV^H}$ [17], where ^{H} denotes Hermitian transpose. Fig. 2 depicts the magnitude-ordered singular values of $\boldsymbol{R}$ for several simulation and measurement scenarios of an active antenna whose details are disclosed in Section IV. The simulations are performed with different levels of Signal to Noise Ratio (SNR) according to:

$$\text{SNR} = -20log_{10}\left(\frac{||\boldsymbol{b}' - \boldsymbol{b}||_2}{||\boldsymbol{b}||_\infty}\right) \tag{8}$$

where the primed vector $\boldsymbol{b}'$ contains the noise-contaminated observations, and the infinity norm performs a normalization of the error with respect to the maximum of the near-field. By the properties of SVD, (7) has a unique solution if only the last singular value σ_M is equal to zero. In a practical measurement case, σ_M has a level comparable to the noise floor of the measurement, as shown in the simulation scenarios of Fig. 2. The corresponding singular vector V_M solves (7) with a comparable accuracy level to the noise floor.

If the noise floor of the system is too high, it becomes impossible to distinguish σ_M from the rest of singular values leading to the existence of multiple solutions for (7). This does not mean that any of those solutions is valid because there is no guarantee that they meet the non-convex constraint $|\boldsymbol{\psi_1}| = 1$. Therefore, successful phase retrieval is only guaranteed when the noise floor of the system is lower than all singular values of $\boldsymbol{R}$.

The Conjugate Gradient (CG) [20] algorithm is proposed to retrieve the solution vector $\boldsymbol{\psi_1}$ when the SVD analysis gives multiple solutions with $|\boldsymbol{\psi_1}| \neq 1$. In an effort to relax the non-convex condition of unitary magnitude, the linear system (7) is constrained with the condition that one of the entries of $\boldsymbol{\psi_1}$ should be 1 [18]. The benefit of using an iterative algorithm lies on its inherent regularization properties, looking for vectors with the minimum norm. This helps to filter out solution vectors with very strong amplitude variance. The initial guess for the CG is an all-ones vector and the algorithm is stopped when the residual of the last iteration achieves a level similar to the estimated noise floor of the system. The resulting solution vector is likely to not feature entries of unit magnitude. Therefore, only the phase of this vector is extracted and used as initial guess of a new CG algorithm. This process is repeated multiple times until the variations between subsequent CG evaluations stagnate.

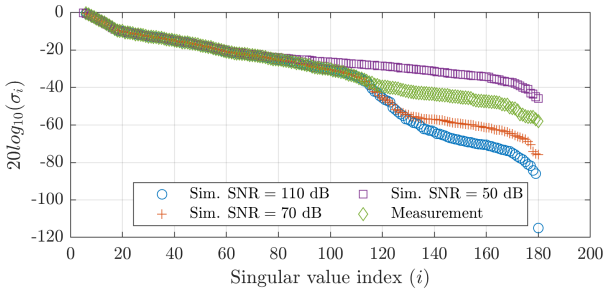

Fig. 2. Singular values of $\boldsymbol{R}$ for several simulations and measurement scenarios.

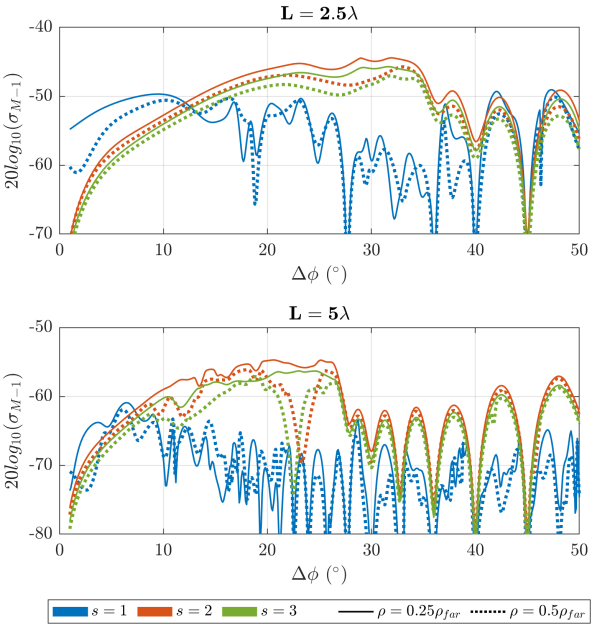

Fig. 3. Magnitude of σ_{M-1} for several simulation parameters.

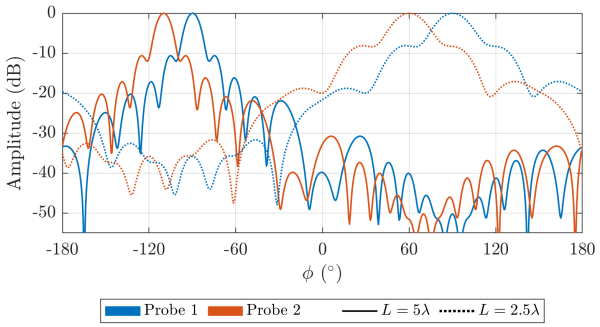

Fig. 4. Near-field signals of one of the conducted simulations. The patterns for different values of L have been shifted 90º away of each other only here for better visualization.

III. Numerical results

A. Uniqueness of the phase retrieval

The uniqueness of the linearized approach is assessed by computing the level of the second to last singular value σ_{M-1} under noise-free conditions. The higher this value the more chances of maintaining uniqueness in the presence of noisy data. For example, a level of $\sigma_{M-1} = -50$ dB means that the uniqueness of the linearized approach is compromised when the measurement is contaminated with error signal levels higher than -50 dB.

An analytical near-field measurement scenario is simulated using dipole-based antennas. The AUT is a $L \times L$ array of Huygens sources fed with uniform amplitude and phase and $\hat{z}$ polarization. The antenna is centered in the coordinate system origin over the YZ plane with the main beam pointing along $\hat{x}$. Two ideal Hertz probes on the XY plane with an angular separation $\Delta\phi$ measure the near-field in a single-cut of radius ρ in M sampling points each. The use of alternate polarizations between probes has shown to be beneficial for the phase retrieval [19]. However, single-cut measurements are known to be unreliable for the cross polarized field components. Therefore, all the studies will be conducted with the Hertz dipoles oriented along $\hat{z}$ to consider only the copolar component of the fields.

The linearized phase retrieval approach is evaluated for different combinations of $\Delta\phi$ and ρ. Fig. 3 depicts the magnitude of σ_{M-1} of each combination for $L = 2.5\lambda$ and 5λ. Highest levels of σ_{M-1} are obtained for angular separations of around 30º and 20º for $L = 2.5\lambda$ and 5λ, respectively. To better understand the behaviour of these parametric curves, Fig. 4 shows the near-field for $\Delta\phi = 30$º and 20º for $L = 2.5\lambda$ and 5λ, respectively, and a measurement radius of 25% the far-field distance of the AUT ($\rho = 0.25\rho_{far}$).

The proposed formulation does not impose any requirement relating the number of samples and probe angular separation. An oversampling ratio with respect to complex single-cut measurements has been defined as $s = M/(2N+1)$. For $s = 1$ low levels of σ_{M-1} are obtained because there are not enough samples so the operator $\boldsymbol{H}\boldsymbol{H}^{\dagger}$ is able to perform a proper modal filtering. Better performance is obtained with $s = 2$ which is a typical value of phaseless measurements [12]. Unlike in conventional phaseless retrieval approaches, the number of unknowns in this approach is equal to the number of measurement points. As a result, too high levels of oversampling can lead to slightly worse stability, because the algorithm needs to retrieve more absolute phase samples. This explains the slight degradation when s increases to 3.

When the probes are too close to each other, $\boldsymbol{\psi_{2,1}}$ will exhibit a low dynamic range leading to a bad conditioning of the system. Inversely, when $\Delta\phi$ increases too much the amplitude ratio between $|\boldsymbol{b_1}|$ and $|\boldsymbol{b_2}|$ becomes too large degrading the performance. This is specially problematic when the main lobe is scanned by one probe while the other is measuring a pattern null. When this happens, the magnitude of σ_{M-1} decreases considerably, leading to the multiple lobe-null pattern observed for large $\Delta\phi$ values in Fig. 3. The near-field pattern of common antennas exhibit shallower nulls and slower angular variations than in the far-field. Hence, low values of ρ mitigate the aforementioned bad conditioning issues, which is reflected on smoother curves and slightly higher values of σ_{M-1}.

B. Influence of probe imbalances

The experiment conducted in Section III.A shows that the values of σ_{M-1} are in the order of -50 dB in most cases. This value is usually lower than the uncertainty provided by common measurement facilities [21] and the error of the single-cut approximation [3]. As a result, uniqueness condition will be hardly met in a practical case and the accuracy of the retrieved solution will be degraded. This degradation has been analyzed in a previous publication [11]. On this section the analysis is extended to the uncertainties specific of the two-probe set-up: channel balance, angular separation and radial displacement between the probes. A metric ε is defined as the mean square error of the reconstructed near-field of the first probe:

$$\varepsilon = \frac{\left|\left||\boldsymbol{b_1}| \otimes \tilde{\boldsymbol{\psi}}_{\boldsymbol{1}} - |\boldsymbol{b_1}| \otimes \boldsymbol{\psi_1}\right|\right|_2^2}{M||\boldsymbol{b_1}||_\infty^2} \tag{9}$$

where $\tilde{\boldsymbol{\psi}}_{\boldsymbol{1}}$ denotes the retrieved solution from (7) to differentiate it from the ground truth $\boldsymbol{\psi_1}$.

The simulations of Section III.A have been repeated introducing several distortions to the near-field data:

1) Probe separation: An imperfect characterization of this parameter is emulated. The nominal separation $\Delta\phi$ is used to generate $\boldsymbol{H}$; but matrix $\boldsymbol{B}$, which contains the measured near-field data, is generated with an erroneous separation $\Delta\phi'$.

2) Channel imbalance: The signal measured by the probes may suffer different levels of attenuation and phase delay on the receiver interface. Variations in the probe gain, cable length and measurement distance are the main contributing factors to this uncertainty. An

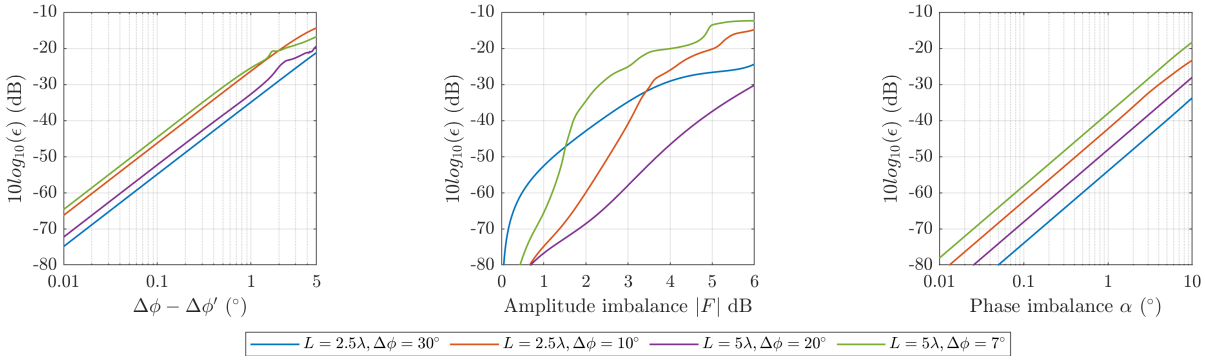

Fig. 5. Effects of the two-probe system uncertainties on the retrieved solution.

imperfect channel balance is emulated weighting $\boldsymbol{b_2}$ with a complex factor $F = |F|e^{j\alpha}$.

Fig. 5 depicts ε for the different error sources for the case $\rho = 0.25\rho_{far}$. The angular separation and phase imbalance errors heavily impact the accuracy of the phase retrieval. For example, an uncertainty in the determination of the probe angular separation of 1° can introduce errors up to -25 dB. A similar error level would be introduced by an uncertainty of 3 dB or higher for the amplitude imbalance, which indicates the technique is more robust against this type of mismatches.

For the phase imbalance and probe pointing, the curves exhibit the same ordered sequence in terms of robustness against imbalances (blue is the most robust and green the least). Using the data of Fig. 3, the σ_{M-1} values for the scenarios represented by the blue, purple, red and green are roughly -45, -53, -57 and -64 dB, respectively. They follow the same sequence, thus confirming the relation between the magnitude of σ_{M-1} and robustness against imbalances.

IV. Phaseless antenna measurements

The proposed technique is evaluated in the anechoic chamber of the Technical University of Madrid (UPM). A spherical near-field measurement range is used to perform single-cut measurements of a 30 GHz 8×8 circular patch array [22] with linear polarization at a measurement distance of 3 m ($0.7\rho_{far}$). The electrical size of the complete antenna is around $10\lambda \times 10\lambda$, which yields a truncation index $N = 42$. The array is connected to an integrated circuit that controls each of the 8 patch columns individually, so different radiation pattern configurations can be generated:

1) Configuration 1: The 4 central columns are fed with uniform amplitude and phase and the rest are switched off.

2) Configuration 2: All 8 columns are fed with uniform amplitude and phase.

3) Configuration 3: Same as configuration 1 but a linear phase shift is applied to generate a 30º beam steering.

The probe system is composed by a conical and a rectangular horn mounted in a metallic supporting structure separated 30 cm from each other. The AUT and probes are vertically polarized and only copolar measurements will be conducted. Fig. 6 shows the AUT and probe system mounted in the anechoic chamber. The resulting $\Delta\phi$ is around 6º, which is large enough to obtain phase diversity, but smaller than the -10 dB beam-width avoiding the multi null-lobe pattern of Fig. 3. Both probes are connected to the receivers A and B of a PNA-X N5264A [23]. The AUT is fed by a external synthesizer which is also connected through a coupler to receiver R of the PNA-X. This configuration allows to measure absolute and relative phases of the probes.

The strict requirements of phase and probe separation imbalances pose a challenge when implementing the proposed technique. No effort has been made to ensure channel equalization on the cables connecting the probes with the measurement receiver. In addition, the horns have different radiation patterns. Probe pattern correction could be incorporated by weighting the SCWC of the AUT with those of the probe in eqs. (1-2) and its discrete versions [4]. In the present measurement scenario both probes illuminate the AUT over a 1º angular sector, so probe pattern effect can be neglected and such correction has not been implemented. Nevertheless, the different levels of directivity and phase center contribute to the channel imbalance, which cannot be neglected. Therefore, an advanced calibration technique is proposed to quantify and correct with high accuracy all these imbalances. After the chamber has been calibrated for a given two-probe configuration, multiple phaseless measurements can be performed with the proposed linearized approach.

A. Probe-to-probe calibration

This step requires the measurement in a single-cut of an auxiliary antenna with access to a reference channel so amplitude and phase can be acquired. The measured complex signals $\boldsymbol{b_1}$ and $\boldsymbol{b_2}$ are used to compute the SCWC of the auxiliary antenna inverting (3) and (4). The SCWC obtained from the first and second probe are denoted $\boldsymbol{c_n^{(1)}}$ and $\boldsymbol{c_n^{(2)}}$ respectively.

The angular separation $\Delta\phi$ in the near-field is reflected as a linear phase shift in the SCWC domain. Computing the slope of the phase shift between $\boldsymbol{c_n^{(1)}}$ and $\boldsymbol{c_n^{(2)}}$ offers and accurate way of finding the value of $\Delta\phi$. Once the linear slope is cancelled the amplitude and phase imbalances between probes are computed by taking the average of the ratio between both sets of coefficients.

A standard gain horn was used as the auxiliary antenna. The obtained $\Delta\phi$, $|F|$ and α were 5.73º, -0.89 dB and 3.32º, respectively. After the equalization of the near-field patterns, differences of -40 dB between them were observed, which are in the level of typical antenna measurement uncertainties. However, this uncertainty levels seem too high to guarantee the uniqueness according to the studies of Section III.A.

B. AUT measurement

The 8×8 array is mounted on the positioner and a two-probe single-cut measurement is performed to obtain the complex signals $\boldsymbol{b_1}$ and $\boldsymbol{b_2}$ using Configuration 1. The scanning is performed with an angular step of 2º so that $M = 180$. A new set of calibration coefficients was computed for the measurement, with values of 5.7º, -0.93 dB and 3.34º confirming the validity of the calibration independently of the antenna. However, this latter values were discarded

and the ones of the auxiliary antenna were used for the subsequent steps to emulate a true phaseless measurement.

From the near-field data, the signals $|\boldsymbol{b_1}|$, $|\boldsymbol{b_2}|$, $\boldsymbol{\psi_{2,1}}$ are extracted and the linearized system is constructed considering the calibration coefficients. The corresponding singular value distribution is the green curve of Fig. 2. The same plot contains the SVD of synthetically generated measurements using the complex data of the AUT. Only for SNR $=$ 110 dB a magnitude gap in the SVD distribution can be distinguished, showing that $\sigma_{M-1} \approx -90$ dB. The equivalent noise floor of the measurement is well above this level, which indicates that the uniqueness condition is not met for the measurement data.

The system is solved taking the last singular vector V_M (SVD approach) and with the Conjugate Gradient using as starting point a vector of ones (CG approach). Fig. 7 depicts the amplitude and phase of $\tilde{\boldsymbol{\psi}}_{\mathbf{1}}$ retrieved with both techniques. The SVD method is equivalent to a matrix inversion and the magnitude of this vector is far from constant which is an indication of a poor linearization result. With CG a flatter amplitude response is obtained thanks to its regularization properties. For both methods the phase of $\tilde{\boldsymbol{\psi}}_{\mathbf{1}}$ exhibits good agreement with the true near-field phase close to boresight, but for the SVD approach the error increases considerably for larger ϕ angles.

The near-field vector is obtained combining the measured amplitude with the retrieved phase of the first probe: $\boldsymbol{b_1} = |\boldsymbol{b_1}| \otimes \tilde{\boldsymbol{\psi}}_{\mathbf{1}} \oslash |\tilde{\boldsymbol{\psi}}_{\mathbf{1}}|$, where $\oslash$ indicates element wise division. Such division is generally needed since the solution vector is likely to not feature entries of unit magnitude. The transformed far-field has been depicted in Fig. 8 along with the reference far-field computed using complex data. The same measurement and postprocessing steps are repeated for Configuration 2 and 3. The amplitude agreement is excellent in all cases but the complex error [12] reveals the imperfect phase reconstruction. For the CG method the error is in the order of -30 dB, while the SVD techniques shows higher values indicating an unreliable phase retrieval like in the near-field case. Phase retrieval of beam steering antennas becomes challenging because their lack of symmetry leads to more chances of falling in local minima [12]. This explains the higher errors observed in Configuration 3. However, the amplitude agreement is still good.

C. Comparison with other methods

To better demonstrate the potential of the proposed technique, two previously proposed phase retrieval methods are challenged with the measured near-field data of Configuration 1. The details of their implementation can be found in our previous publications [9]–[11].

The first one consists on an iterative propagation of the complex field back and forth between two measured single-cuts [9], [10]. It is inspired on the well-known Gerchberg–Saxton technique used in planar and spherical phaseless measurements [13]. For its implementation, the near-field of the first probe is used to compute a synthetic measurement at a distance of 2 m. Then, the algorithm can be evaluated iterating between the fields at 2 m and 3 m.

The second method formulates the phase retrieval as non-linear minimization to find the SCWC that radiate the near-field amplitude of the two probes [11]. Therefore, no partial coherence or multiple distance information is incorporated to the algorithm. The minimization problem is tackled with a non convex solver employing Wirtinger Flow derivatives [24].

Fig. 9 depicts a comparison of the far-field pattern retrieved by the different solvers. For the linearized approach, only the CG solution has been depicted. The iterative solver is capable of reconstructing

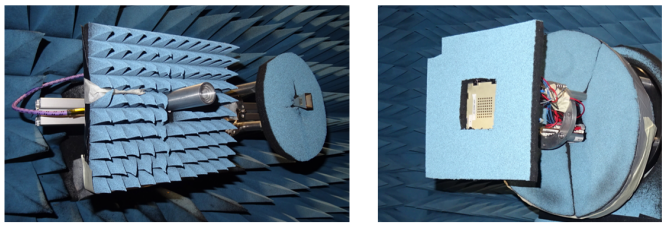

Fig. 6. Two-probe arrangement (left) and AUT (right) used for the anechoic chamber measurements .

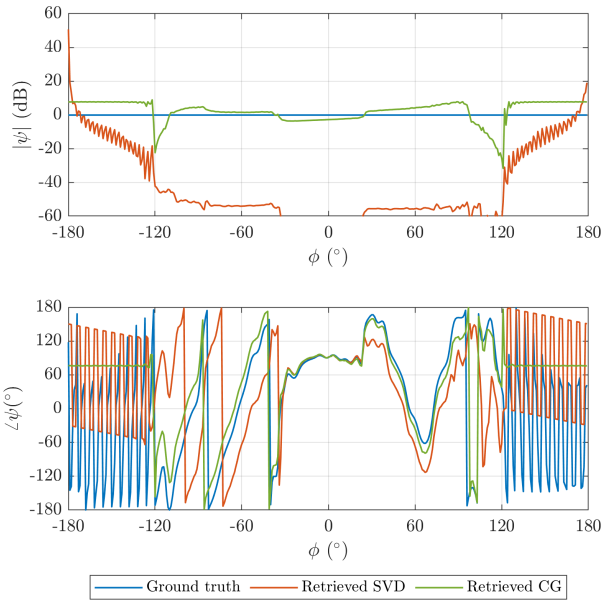

Fig. 7. Magnitude and phase of the solution $\tilde{\boldsymbol{\psi}}_{\mathbf{1}}$. Ground truth is a vector of magnitude one containing the phase of the signal measured by the first probe.

the amplitude pattern with good accuracy but the phase reconstruction fails. This is not a surprising behaviour, since this technique has been shown to fall frequently into sub-optimal solutions [12]. The non-convex solver fails to reconstruct both amplitude and phase, showcasing the well-known limitations of single-scan phaseless measurements. Despite providing the solver with the near-field data from two different probes, the two signals are virtually shifted copies of each other, as show in Fig. 4. Two uncoherent probe measurements are not enough to reconstruct the phase because the inversion problem becomes highly undetermined. Only with the relative phase between the probes new information is incorporated to the solver.

V. Conclusion

The implementation of a linearized phaseless single-cut measurement technique with reduced hardware requirements has been reviewed. A measurement set up with two probes connected to the same receiver is proposed to extract partial coherence information of the near-field. Simulation results show that the phase retrieval is guaranteed under high accuracy conditions. The uncertainties of real antenna measurements compromise this uniqueness condition. A conjugate gradient approach is proposed to retrieved the absolute phase information with improved accuracy respect to a direct matrix inversion. In addition, it has been shown how a practical calibration process can lead to accurate near-field to far-field transformation of the single-cut fields. This has been validated with a phased array antenna in different configurations.

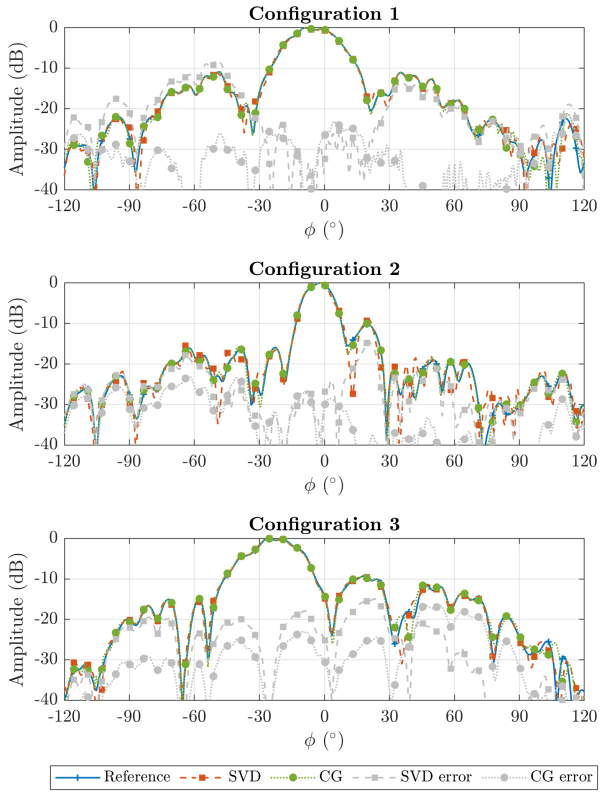

Fig. 8. Far-field reconstruction of the linearized matrix inversion techniques.

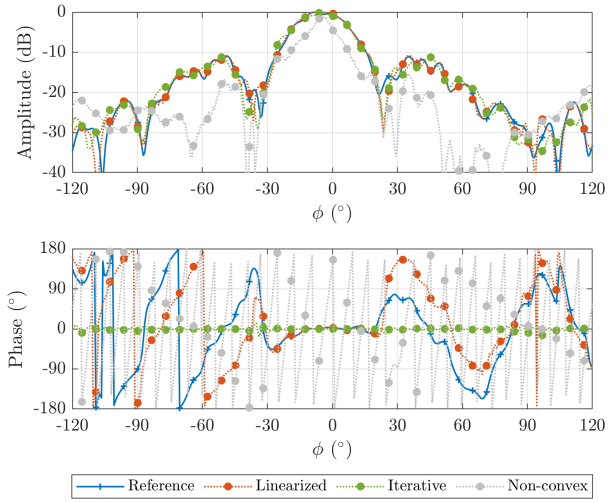

Fig. 9. Far-field reconstruction from the different phase retrieval solvers.

REFERENCES

[1] S. Omi, T. Uno, T. Arima, "Single-Cut Near-Field Far-Field Transformation Technique Employing Two-Dimensional Plane-Wave Expansion", in *IEEE Antennas and Wireless Propagation Letters*, vol. 17, no. 8, pp. 1538-1541, Aug. 2018.

[2] Y. Sugimoto, H. Arai, T. Maruyama, M. Nasuno, M. Hirose, S. Kurokawa, "Fast Far-Field Estimation Method by Compact Single Cut Near-Field Measurements for Electrically Long Antenna Array", *in IEEE Trans. Antennas Propag*, vol. 66, no. 11, pp. 5859-5868, Nov. 2018.

[3] R. Cornelius, T. Salmerón-Ruiz, F. Saccardi, L. Foged, D. Heberling, M. Sierra-Castañer, "A comparison of different methods for fast single-cut near-to-far-field transformation", in *IEEE Antennas and Propagation Magazine*, vol. 56, no. 2, pp. 252-261, Apr. 2014.

[4] T. Salmerón-Ruiz, M. Sierra-Castaner, F. Saccardi, S. Burgos, F. J. Cano-Fácila, Lars J. Foged, "A Fast Single Cut Spherical Near-Field-to-Far-Field Transformation Using Cylindrical Modes" in *2014 8th European Conference on Antennas and Propagation (EuCAP)*, 2014.

[5] "IEEE Recommended Practice for Near-Field Antenna Measurements," in *IEEE Std 1720-2012*, pp.1-102, 5 Dec. 2012.

[6] "IEEE Standard Test Procedures for Antennas," in *ANSI-IEEE Std 149-1979*, vol., no., pp.1-144, 30 Nov. 1979

[7] J. E. Hansen, "Spherical Near-Field Antenna Measurements", London, U.K.: Peter Peregrinus, 1988.

[8] R. Tena Sanchez, M. Sierra Castaner and L. J. Foged, "A Referenceless Antenna Measurement System Based on Software-Defined Radio [Measurements Corner]," in *IEEE Antennas and Propag. Magazine*, vol. 62, no. 5, pp. 108-118, Oct. 2020, doi: 10.1109/MAP.2020.3012897.

[9] F. R. Varela, B. Galocha Iragüen, M. S. Castañer, "Single-Cut Phaseless Near-Field Measurements for Fast Antenna Testing," in *IEEE Trans. Antennas Propag.*, vol. 70, no. 10, pp. 9994-9999, Oct. 2022.

[10] F. R. Varela, B. G. Iragüen, M. S. Castañer, "Single-Cut Phaseless Near-Field to Far-Field Transformation", *2022 16th European Conference on Antennas and Propagation (EuCAP)*, Madrid, Spain, 2022.

[11] F. R. Varela, B. Galocha Iragüen, M. S. Castaner, "Single-Cut Phaseless Near-Field Measurements using Specialized Probes", *2022 Antenna Measurement Techniques Association Symposium*, Denver, CO, USA.

[12] F. R. Varela, J. F. Álvarez, B. G. Iragüen, M. S. Castañer, O. Breinbjerg, "Numerical and Experimental Investigation of Phaseless Spherical Near-Field Antenna Measurements", in *IEEE Trans. Antennas Propag.*, vol. 69, no. 12, pp. 8830-8841, Dec. 2021.

[13] N. Mézières, L. Le Coq, "Improvement of the Gerchberg–Saxton Algorithm Convergence in Phaseless Antenna Measurements via Spherical-Wave Filtering", in *IEEE Trans. Antennas Propag.*, vol. 71, no. 5, pp. 4540-4545, May 2023

[14] B. Fuchs, M. Mattes, S. Rondineau, L. Le Coq, "Phaseless Near-Field Antenna Measurements From Two Surface Scans — Numerical and Experimental Investigations", in *IEEE Trans. Antennas Propag.*, vol. 68, no. 3, pp. 2315-2322, March 2020.

[15] S. Costanzo, G. Di Massa, "An integrated probe for phaseless plane-polar near-field measurements", *Microw. Opt. Technol. Lett.*, vol. 30, no. 5, pp. 293–295, 2001.

[16] S. Costanzo, G. Di Massa, and M. D. Migliore, "A novel hybrid approach for far-field characterization from near-field amplitude-only measurements on arbitrary scanning surfaces", *IEEE Trans. Antennas Propag.*, vol. 53, no. 6, pp. 1866–1874, Jun. 2005.

[17] J. Kornprobst, A. Paulus, J. Knapp and T. F. Eibert, "Phase Retrieval for Partially Coherent Observations", in *IEEE Transactions on Signal Processing*, vol. 69, pp. 1394-1406, 2021.

[18] A. Paulus, J. Knapp, J. Kornprobst and T. F. Eibert, "Reliable Linearized Phase Retrieval for Near-Field Antenna Measurements with Truncated Measurement Surfaces", in *IEEE Trans. Antennas Propag*, vol. 70, no. 8, pp. 7362-7367, Aug. 2022.

[19] J. Kornprobst, A. Paulus, J. Knapp and T. F. Eibert, "Multi-Probe Array Design for Partially-Coherent Phase Retrieval in Near-Field Measurements", *2023 17th European Conference on Antennas and Propagation (EuCAP)*, Florence, Italy, 2023.

[20] Y. Saad, *Iterative Methods for Sparse Linear Systems*, Philadelphia, PA, USA:SIAM, 2003.

[21] M. A. Saporetti et al, "International Facility Comparison Campaign at L/C Band Frequencies", *2017 Antenna Measurement Techniques Association Symposium*, Atlanta, GO, USA.

[22] A. T. M. Barrado et al,"Evaluation of a Planar Reconfigurable Phased Array Antenna Driven by a Multi-Channel Beamforming Module at Ka Band," in *IEEE Access*, vol. 9, pp. 63752-63766, 2021.

[23] N5264A PNA-X Measurement Receiver Product Fact Sheet. https://www.keysight.com/es/en/assets/7018-01930/flyers/5989-9639.pdf (accessed Nov., 2023).

[24] E. J. Candes, X. Li and M. Soltanolkotabi, "Phase Retrieval via Wirtinger Flow: Theory and Algorithms", *IEEE Trans. on Information Theory*, vol. 61, no. 4, pp. 1985-2007, April 2015.